Crystalline Organic Molecular Thin Film with Electrical Switching Property: Scanning Probe Microscopy and Optical Spectroscopy Study

J. C. Li*,† and Z. Q. Xue

Department of Electronics, Peking University, Beijing 100871, People's Republic of China

K. Z. Wang

Department of Chemistry, Beijing Normal University, Beijing 100875, People's Republic of China

Z. M. Wang and C. H. Yan

State Key Lab of Rare Earth Materials Chemistry and Applications, Peking University, Beijing 100871, People's Republic of China

Y. L. Song, L. Jiang, and D. B. Zhu

Organic Solid Lab, Institute of Chemistry, Chinese Academy of Science, Beijing 100080, People's Republic of China

Received: May 25, 2004; In Final Form: October 2, 2004

We report on the growth and characterization of crystalline 1,1-dicyano-2,2-(4-dimethylaminophenyl)ethylene (DDME) thin film with electrical switching property. X-ray diffraction analysis indicates that bulk single-crystal DDME belongs to monoclinic, space group $P2_1$, and $Z = 2$ structure. Optical spectroscopy shows that the film chemical structure is consistent with that of the powder material, suggesting that DDME material is very stable during the vacuum thermal deposition process. Scanning probe microscopy and transmission electron microscopy observations reveal that the as-deposited film has extended crystal structure and smooth surface morphology in micrometer scale. Parallel molecular stacking structure is repeatedly observed in the film surfaces with the axis of the molecular stack parallel to the substrate. The *ac* crystal plane is found to be one of the most stable surfaces of the DDME film in ambient conditions. Nanometer scale data storage is realized on the film by applying pulse voltage between the STM tip and the substrate. The switching mechanism is briefly discussed.

1. Introduction

Organic molecular thin films are extremely attractive due to their adaptability, simplicity, and low cost of manufacturing. These unique advantages make them suitable for potential applications in ultrafast molecular electronic devices and nanoscale data storage.[1−5] Traditionally, organic functional films are made of two or more components. However, the inhomogeneity of different components in the film may result in poorly ordered polycrystalline or even amorphous films with a large density of defects, and consequently leads to poor device performance. In contrast, single-crystal single-component organic thin films can exhibit better electrical/optical properties than their amorphous or polycrystalline multicomponent counterparts.[6] It was suggested that vacuum evaporated crystalline single-component organic molecular thin films could be favorable for potential application to ultrahigh-density data storage.[7] Therefore the reproducible growth of large-scale single-crystal single-component organic thin films with unique electrical/optical properties would be very desirable.

So far, a number of articles have been reported on the observation of electrical switching and memory phenomena in different molecular systems.[8−13] However, the correlation between the film/molecular structural transition and the electrical switching has not been well understood yet. The main reason may be that their relationship is very complicated. In fact, the problem can be broken up into two parts: how the molecules are initially arranged on the substrate before switching and how the film/molecular structure changes when a threshold electrical filed is applied. Consequently, the effect of the structural/phase transitions on the electrical and optical properties of the film is still in question. Obviously, to get a better understanding of the observed phenomena, further investigation of the structural, morphological, electrical, and optical properties of the molecular systems is necessary.

We previously demonstrated that nanoscale data storage could be realized on crystalline single-component 1,1-dicyano-2,2-(4-dimethylaminophenyl)ethylene (DDME) thin film with electrical bistability and parallel molecular stacking structures, although the switching mechanism and the film crystal structure are still not clear.[14] Careful study of the growth, surface morphology, and electrical/optical properties of the film may give some explanations from an experimental view. Thus, in this article, we will focus on the growth and characterization of DDME thin films. The chemical structure of the sample is first characterized by using Raman, Fourier transform infrared (FTIR), and ultraviolet−visible (UV−vis) spectroscopy. The crystal structure and surface morphology are then comparably

† Present address: Department of Chemistry, The University of Chicago. E-mail: jcli@uchicago.edu.

10.1021/jp047733g CCC: $27.50
Published on Web 11/20/2004

investigated with various analyzing techniques. Finally, the switching mechanism is briefly discussed.

2. Experiment Section

The DDME material is designed and synthesized in our lab. Bulk single-crystal DDME with orange color and block shape, suitable for X-ray diffraction analysis, is grown from its supersaturated solution in ethanol/CCl_4 (mole ratio = 1:1) in ambient conditions. X-ray diffraction is performed on a 0.50 × 0.33 × 0.25 mm^3 single crystal, using a NONIUS KappaCCD at temperature of 293 K with $\lambda = 0.71073$ Å. The θ range for data collection is from 4.34 to 27.51°. No more than 3% decrease on F_0 is observed by X-ray exposure during data collection. The structure is determined by direct method and refined by the full-matrix least-squares method.

The DDME film samples are vapor deposited in a high vacuum chamber at a pressure of about 1×10^{-5} Torr with a deposition rate of ~0.1 nm/s. In the case of Au substrate being used, a fresh 100-nm-thick Au film is thermal evaporated onto clean Si(100) at the deposition rate of 0.2 nm/s. Without breaking the vacuum, the DDME film is then deposited onto the Au substrate. The film deposition rate and thickness are monitored by QCM. The substrates are cleaned by using acetone, ethanol, and deionized water, then dried with nitrogen gas.

NT-MDT P47 atomic force microscopy (AFM) and scanning tunneling microscopy (STM) are used to image the samples deposited on freshly cleaved highly ordered pyrolytic graphite (HOPG) substrate in ambient conditions. The STM tip is electrochemically etched from a tungsten wire 0.2 mm in diameter. The transmission electron microscopy (TEM) study is conducted on a JEM-200CX system. FTIR spectroscopy of the film deposited on KBr substrate is investigated by using a Nicolet Magna 750 spectrophotometer. Raman spectra of DDME thin films deposited on Au-coated silicon are measured with a Renishaw System 1000 Raman spectroscope. UV−vis spectroscopy is performed with a Hitachi U-3310 spectrophotometer, using a quartz cell as the reference (or substrate) and pure ethanol as the solvent.

3. Results and Discussion

The molecular structure of DDME is shown in Figure 1a. It is indicated that the molecule is nearly planar with dimensions of about 1.1 nm × 0.45 nm × 0.25 nm. X-ray structural analysis shows that bulk single-crystal DDME belongs to monoclinic, $P2_1$, and $Z = 2$ structure with lattice parameters of $a = 3.997$ Å, $b = 14.062$ Å, $c = 9.545$ Å, $\beta = 100.6°$, and $V = 527.50$ $Å^3$, respectively. The fundamental crystal data are summarized in Table 1 (for details see ref 15). The crystal packing is shown in Figure 1b,c. When viewed along the *a* axis, the interaction between the intermolecular electron donor group and acceptor group is made evident (Figure 1b). When projected along the *b* axis, striking two-dimensional parallel molecular stacks can be clearly seen (Figure 1c).

The FTIR spectra of the film sample are measured.[16] Compared with that of the powder material, there is no big difference in the spectra of the thin film,[17] indicating the thermal stability of DDME material during the deposition process.

UV−vis spectra also confirm that the film has the same chemical structure as that of the powder material. As shown in Figure 2a, the ethanol solutions of both DDME powder and film exhibit one absorption shoulder centered at 272 and one absorption band at 432 nm, respectively. The shoulder at 272 nm is ascribed to the B band of $\pi \rightarrow \pi^*$ excitation of the benzene ring.[18] As reported in the donor−π−acceptor complex materials, the intense and prominent band at 432 nm is assigned to the charge-transfer (CT) transition between intermolecular donor and acceptor groups.[19] UV−vis spectra of various DDME thin films deposited on quartz glass substrate are shown in Figure 2b. The spectra exhibit a strong broad band in the range of 200 to 320 nm centered at about 270 nm. For films thicker

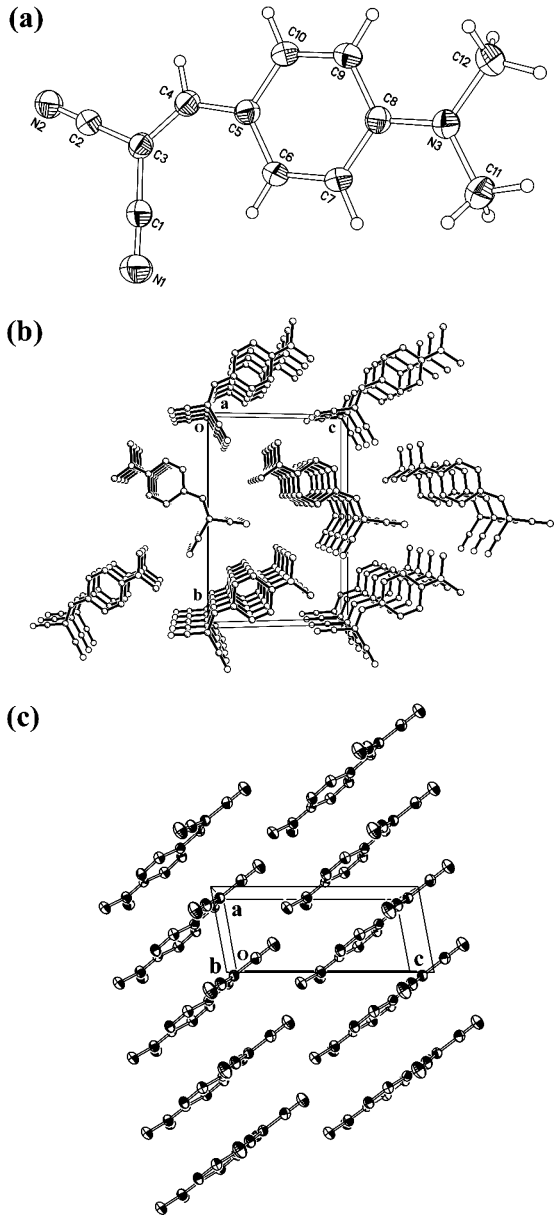

Figure 1. Schematic molecular structure (a) and crystal packing of DDME material (b) viewed along the *a* axis and (c) projected along the *b* axis.

TABLE 1: Selected Crystal Data of the DDME Single Crystal

empirical formula	$C_{12}H_{11}N_3$
formula weight	197.24
crystal system, space group	monoclinic, $P2_1$
unit cell dimensions	$a = 3.9972(4)$ Å, $\alpha = 90°$
	$b = 14.0618(17)$ Å, $\beta = 100.600(7)°$
	$c = 9.5477(11)$ Å, $\gamma = 90°$
volume	527.50(10) $Å^3$
Z, calcd density	2, 1.242 Mg/m^3
abs coeff	0.077 mm^{-1}
F(000)	208
Crystal size	0.50 × 0.33 × 0.25 mm^3
θ range for data collection	4.34−27.51°

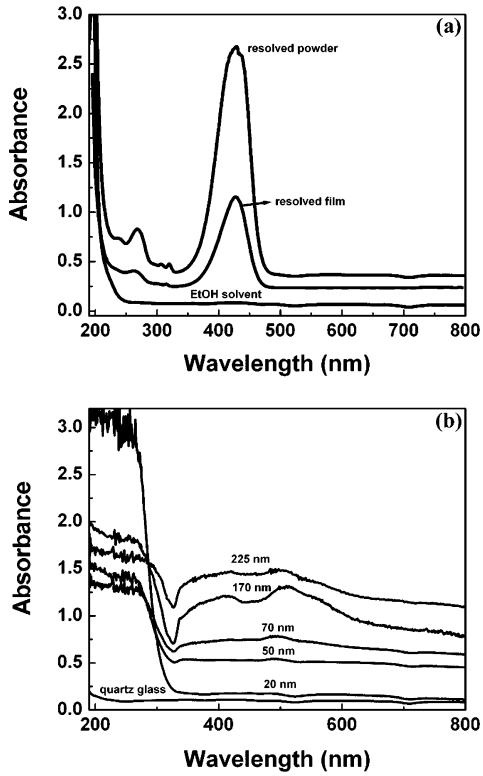

Figure 2. UV−vis spectra of (a) DDME powder and films resolved in pure ethanol and (b) the films deposited on quartz glass slides.

than 70 nm, the spectra show two weak broad bands centered at about 410 and 510 nm, respectively, which may result from the splitting of the 432 nm absorption band shown in Figure 2a. It also indicates that when the film reaches about 100 nm thick, it starts to grow thicker.

The growth and surface morphology of a series of film samples are analyzed with use of tapping mode AFM with a scan rate of 1 Hz. As shown in Figure 3, it is indicated that the films with mass thickness of 20 and 50 nm consist of large branched islands with flat surface features in the micrometer scale. Moreover, as revealed by the inset of Figure 3b, the film surface is characterized with multistep structures. The section analysis indicates that the step height is in the range of 0.485 to 0.679 nm with an average value of about 0.647 nm. The island growth proceeds through the condensation of incoming molecules onto existed nuclei, as can be seen from Figure 3, parts a−e. When the film thickness reaches about 70 nm, top layers begin to form. The islands on the top layer nucleate and grow on the flat surfaces of the bottom layer. As a result, the DDME thin film has a layer-by-layer structure. The islands at the top layer are irregularly bar-shaped and randomly orientated with micrometer lengths and hundred-nanometer thickness. There are a large number of voids left between the islands, though the thicker films are more densely packed. A detailed roughness analysis on these samples is summarized in Table 2.

To verify the film microstructure, TEM observation is carried out on the film samples deposited on a Cu grid precoated with amorphous carbon thin film. Figure 4 shows the representative electron diffraction pattern. It reveals that the film has an extended large-scale single-crystal structure, which would be favorable for nanoscale data storage using tip writing/reading technique.[20] It should be pointed out that the high-voltage electron beam in the TEM system could cause the film to convert from crystalline to amorphous in less than 20 s as that observed in other crystalline organic films.[21]

STM observations are performed on the samples deposited on HOPG substrate in order to get further insight into the film growth mechanism and crystal structure. Figure 5 shows the typical images. The film is shown to be very smooth within a scan area of $2.5 \times 2.5\ \mu m^2$. Note that there exists a groove (∼200-nm wide and 3-nm high) and a step (about 3-nm high) at the top right corner. When the scan size is decreased to a small area, atomic resolution images are observed, confirming that the film has a well-ordered crystal structure. Moreover, unique parallel molecular stacking structures are clearly revealed. The size of the unit building block is about $0.25 \times 0.78\ nm^2$. Similar images are repeatedly observed in the experiments. As indicated by the arrows in Figure 5b, the unit cell ($a \approx 3.8$ Å, $c \approx 9.1$ Å, and their angle $\beta \approx 100.2°$) is quantitatively in agreement with that of the *ac* plane obtained from X-ray diffraction experiments as shown in Figure 2b. This observation suggests that the *ac* crystal plane should be one of the most stable surfaces of the DDME thin film in ambient conditions. It is worthy to note that the axis of the molecular stack is evidently parallel to the HOPG substrate, although the molecular plane may not be perpendicular to the substrate. We know that strong CT interactions usually exist between various electrodes and organic molecules terminated with −CN functional groups.[22] Therefore, it may be reasonable to expect DDME molecules to reside on the HOPG substrate as schematically shown in the inset of Figure 5b. The −CN groups should interact with the HOPG surface, aligning the molecules at an angle. If the angle between the molecular plane and the substrate is about 45°, the molecule will have a projection on the substrate with a size of about $0.23 \times 0.71\ nm^2$, which is just in agreement with that of the STM observation ($0.25 \times 0.78\ nm^2$).

Nanoscale data storage is realized on the thin film by applying a threshold pulse voltage between the STM tip and the HOPG substrate. To prevent possible scratches or other damage to the film, the tip is set to retract a short distance away from the film surface before each pulse voltage is applied (for details see ref 14). As shown in Figure 6, a 2×2 pattern is recorded on the film by setting the STM tip to apply a pulse voltage of 4.7 V, 1 ms along a short distance in the same direction at each position. The pattern can be observed even several hours later, indicating that it is very stable in ambient conditions. Applying negative pulse voltage cannot erase the recorded pattern. On the contrary, similar dots could be recorded on the film by applying negative pulse voltage, using either tungsten or PtIr STM tips.

Electrical switching is observed from the $I-V$ characteristics of DDME thin film measured by STM just before and after recording (Figure 7a). After recording, the film conductance is increased about 3 orders of magnitude. Similar switching behavior is also noted in a microscale Au/DDME/Au sandwich device fabricated on Si(100) substrate with a threshold voltage of about 3.2 V. When the top Au electrode is replaced by a micrometer controlled movable gold tip, after applying threshold voltage, optical microscopy shows that there is a color difference between the as-deposited and the switched regions of the sample (with a good device rate of about 5%). Furthermore, as indicated by Figure 7b, micro-Raman spectra show that there exists a 10 cm^{-1} red shift in the $-C\equiv N$ absorption peak of the recorded area. This may imply that some charge transfer may have taken place in the film during the recording process.[14]

The above results suggest that the electrical switching should result from intrinsic property changes of DDME thin films induced by the applied pulse voltage. In our view, this can be explained using several different approaches. One possible

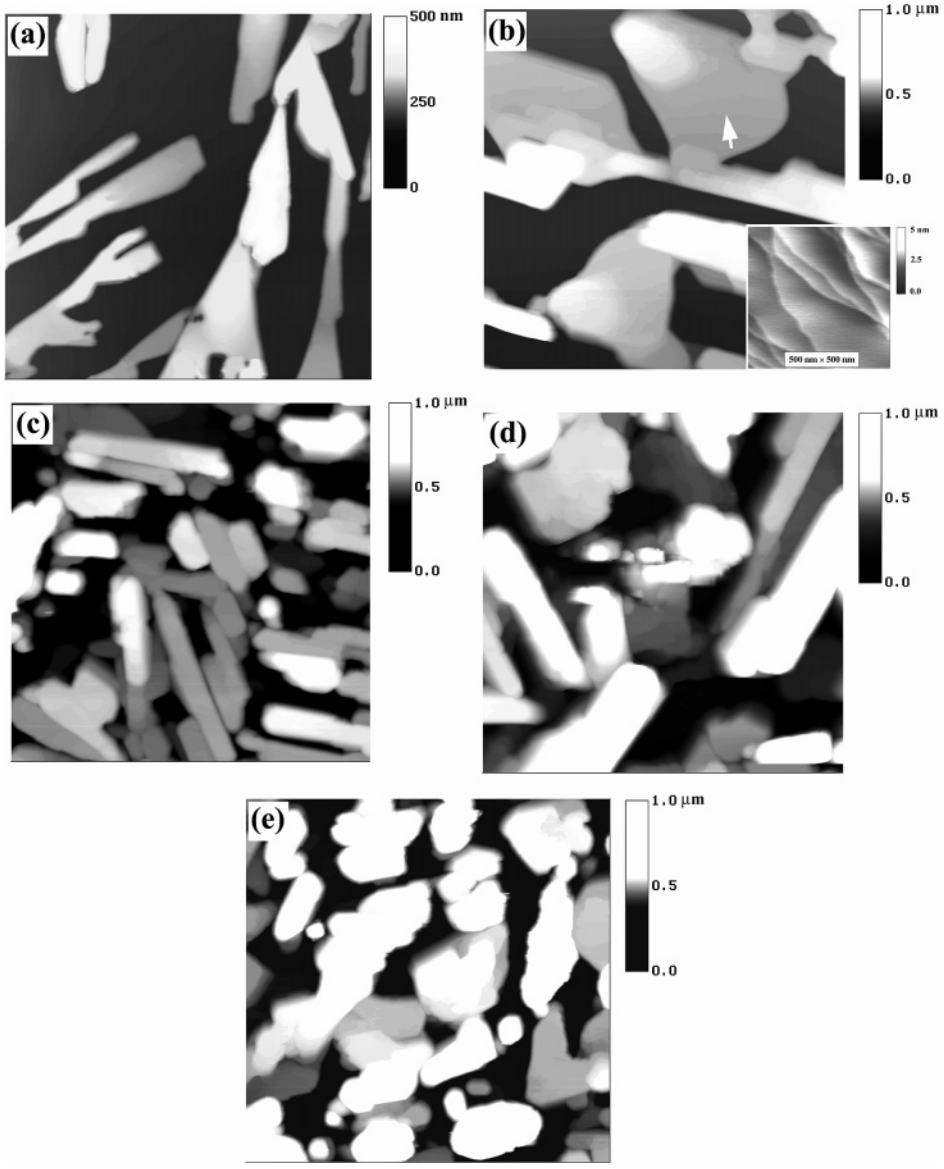

Figure 3. Tapping mode AFM images ($10 \times 10\ \mu m^2$) of DDME thin films with various thickness: (a) 20, (b) 50, (c) 100, (d) 170, and (e) 225 nm, respectively. High-resolution image revealing multistep surface features with a step height in the range of 0.485 to 0.679 nm (inset).

TABLE 2: Summary of the Root-Mean-Square (rms), Average (R_a), and Maximum (R_{max}) Roughness Analysis of the DDME Thin Films Studied in This Work

film thickness (nm)	rms (nm)	R_a (nm)	R_{max} (nm)
20	61	52	309
50	76	60	492
100	141	106	1007
170	172	138	1192
225	165	123	1014

explanation is that the pulse voltage induces CT excitation between the donor and acceptor groups of DDME molecules in the neighboring layers.[19,23−25] This can be schematically described as the following equation

$$(\mathrm{DDME})_{2n} \xrightarrow{E_T} (\mathrm{DDME}^{\oplus} + {}^{\ominus}\mathrm{DDME})_n$$

Neutral high-resistance state — Ionized low-resistance state

with E_T denoted as the threshold applied electrical field, which provides the energy promoting the local nanoscale area from ground state (with lower energy but high resistance) to excited state (with higher energy but low resistance).[26] When the CT excitation interacts with the STM tip or another excited state, the local DDME molecules may be ionized and delocalized.[27] Thus electrical switching is observed. In our case, this process is not reversible by applying a reversed threshold electrical field.

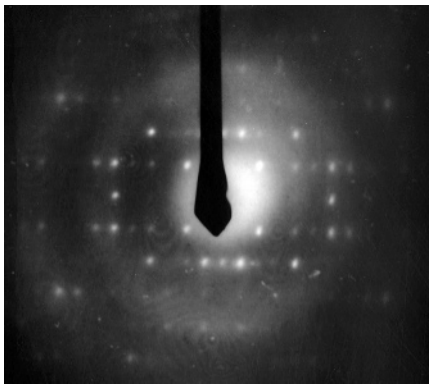

Figure 4. TEM electron diffraction pattern showing that the DDME thin film is well crystallized.

Another reasonable interpretation is that the applied electric field may also induce some structural or phase changes in the

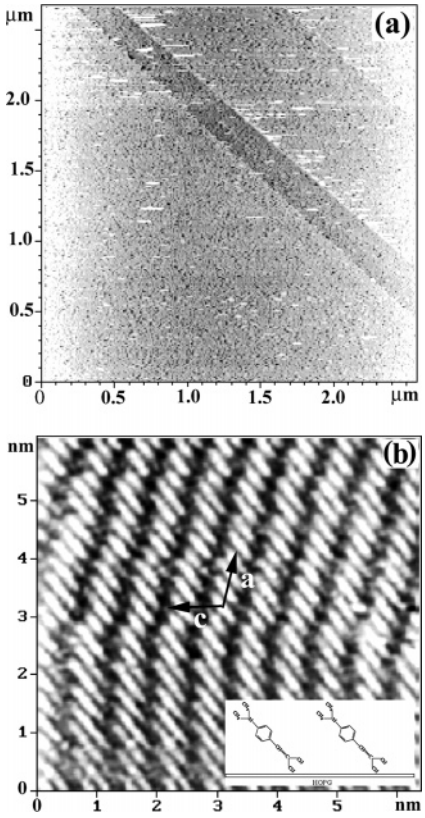

Figure 5. STM images of the DDME thin film deposited on HOPG substrate. STM works at (a) constant current mode with set points of $V_b = 1.007$ V and $I_t = 0.044$ nA and (b) constant height mode with set points of $V_b = 0.081$ V and $I_t = 0.226$ nA. As indicated by the arrows, the unit cell ($a = 3.8$ Å, $c = 9.1$ Å, and $\beta = 100.2°$) is in good agreement with that of the *ac* plane of the bulk single crystal. The inset schematically illustrates two molecules residing on the HOPG surface.

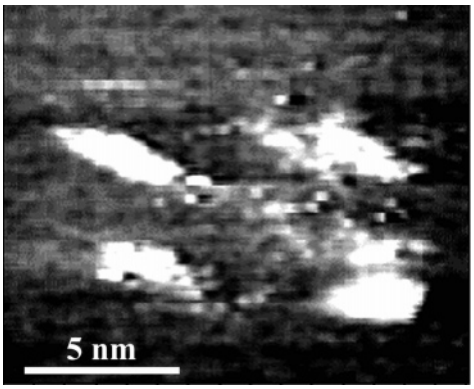

Figure 6. A 2 × 2 nanoscale pattern recorded on the DDME thin film by applying a pulse voltage of 4.7 V, 1 ms between the STM tip and HOPG substrate at each position. STM works at constant current mode with set points of $V_b = 0.873$ V and $I_t = 0.113$ nA.

local region of the film,[2,28,29] which could explain the stability of the low-resistance state after switching. As we know, the lifetime of a CT excitation is very short (normally at the time scale of ms to μs).[23] If there is only a CT excitation but no other changes in the local region when a pulse voltage is applied, the low-resistance excited state should be unstable.[30−32] On the other hand, the electrochromic property of the DDME thin film also indicates the existence of some structural or phase transitions in the local area when a threshold pulse voltage is applied.

Charge trapping/detrapping and unintended doping/dedoping are usually thought to be responsible for the switching properties

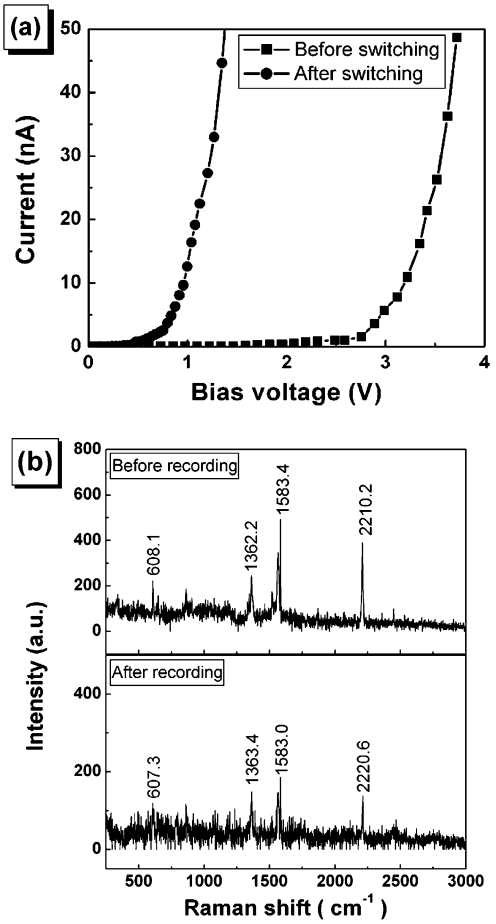

Figure 7. Typical $I-V$ characteristics measured by STM (a) and micro-Raman spectra (b) of the DDME film before and after recording.

in some molecular systems.[12,32,33] In our case, the switching should not result from charge trapping. Otherwise, applying negative pulse voltage will detrap the charge and thus erase the recorded patterns. The possibility of unintended doping/dedoping can be excluded as well, since there are no embedded metal elements in our samples.

The DDME thin film may be initially in a neutral state with high resistance. When an electrical field is applied, there appear to be three possible results. First, if the field is below a threshold value, i.e., the applied electric field is too low to induce structure/phase transitions, the film will keep its original state, though CT excitation may take place in this process. Second, if the electrical field exceeds a key point, i.e., the electric field is enough to induce not only CT excitation but also film structure/phase transitions, the local film may convert to a stable low-resistance state, and thus switching and memory phenomena could be observed. Finally, in an extreme case, if the applied electrical field is too high, the local area may be damaged. At this time, we could not give a more detailed account on the charge-transfer and structural/phase changes in the film.

4. Conclusion

In summary, the structural, morphological, and optical/electrical properties of crystalline DDME thin films are investigated. Bulk single-crystal DDME belongs to monoclinic, $P2_1$, and $Z = 2$ structure. We experimentally demonstrate that crystalline DDME thin films with large-scale smooth morphology could be grown on HOPG substrate by vacuum vapor deposition. The material is found to be very stable during the

deposition process. Parallel molecular stacking structures are observed in the experiments with the stacking axis parallel to the substrate surface. The *ac* crystal plane is found to be one of the most stable film surfaces in ambient conditions. The film exhibits good electrical bistability. Nanoscale data can be recorded on the film by applying pulse voltage between the STM tip and the HOPG substrate. The switching mechanism is ascribed to a transition, from high-resistance state to low-resistance state, resulting from intermolecular charge transfer and film structure/phase transitions induced by threshold applied pulse voltage.

Acknowledgment. We thank Dr. David L. Arrington for his valuable suggestions. The authors wish to thank the financial support from NNSFC (grants no. 20371008 and no. 60231010).

Supporting Information Available: Typical TEM image and electron diffraction pattern of DDME film deposited on a Cu grid precoated with an amorphour carbon film. This material is available free of charge via the Internet at http://pubs.acs.org.

References and Notes

(1) Sohn, L. L. *Nature* **1998**, *394*, 131.
(2) Fujita, W.; Awaga, K. *Science* **1999**, *286*, 261.
(3) Ziemelis, K. *Nature* **1998**, *393*, 619.
(4) Fujii, A.; Yoneyama, M.; Ishihara, K.; Maeda, S.; Murayama, T. *Appl. Phys. Lett.* **1992**, *62*, 648.
(5) Xiong, Z. H.; Wu, D.; Vardeny, Z. V.; Shi, J. *Nature* **2004**, *427*, 821.
(6) Schoonveld, W. A.; Vrijmoeth, J.; Klapwijk, T. M. *Appl. Phys. Lett.* **1998**, *73*, 3884.
(7) Burrows, P. E.; Forrest, S. R. *Appl. Phys. Lett.* **1993**, *62*, 3102.
(8) Bandyopadhyay, A.; Pal, A. J. *Appl. Phys. Lett.* **2004**, *84*, 999.
(9) Moller, S.; Perlov, C.; Jackson, W.; Tausslg, C.; Forrest, S. R. *Nature* **2003**, *426*, 166.
(10) Qu, H. W.; Yao, W.; Garcia, T.; Zhang, J. D.; Sorokin, A. V.; Ducharme, S.; Dowben, P. A.; Fridkin, V. M. *Appl. Phys. Lett.* **2003**, *82*, 4322.
(11) Wu, H. M.; Song, Y. L.; Du, S. X.; Liu, H. W.; Gao, H. J.; Jiang, L.; Zhu, D. B. *Adv. Mater.* **2003**, *15*, 1925.
(12) Li, C.; Fan, W.; Lei, B.; Zhang, D. H.; Han, S.; Tang, T.; Liu, X. L.; Liu, Z. Q.; Asano, S.; Meyyappan, M.; Han, J.; Zhou, C. W. *Appl. Phys. Lett.* **2004**, *84*, 1949.
(13) Gao, X.-C.; Zou, D.-C.; Fujita, K.; Tsutsui, T. *Appl. Phys. Lett.* **2002**, *81*, 4508.
(14) Li, J. C.; Xue, Z. Q.; Li, X. L.; Liu, W. M.; Hou, S. M.; Song, Y. L.; Jiang, L.; Zhu, D. B.; Bao, X. X.; Liu, Z. F. *Appl. Phys. Lett.* **2000**, *76*, 2532.
(15) Wang, K. Z.; Wang, Z. M.; Yan, C. H. *Acta Crystallogr., Sect. E* **2001**, *57*, o214.
(16) The attributions and absorption peaks of the FTIR spectra are as follows: ν_{as}(CH) (2926, 2862, and 2818 cm^{-1}), ν(C≡N) (2210 cm^{-1}), ν-(CH) (1612, 1543, and 1522 cm^{-1}), ν(C═C) (1567 cm^{-1}), ν(CH_3) (1390 and 1362 cm^{-1}), ν(C−N) (1198 and 1182 cm^{-1}), and δ(C−H) (818 cm^{-1}), respectively.
(17) Wang, K. Z.; Xue, Z. Q.; Ouyang, M.; Wang, D. W.; Zhang, H. X.; Huang, C. H. *Chem. Phys. Lett.* **1995**, *243*, 217.
(18) Jaffe, H. H.; Orchin, M. *Theory and Applications of Ultraviolet Spectroscopy*; John Wiley & Sons: New York, 1962.
(19) McGee, B. J.; Sherwood, L. J.; Greer, M. L.; Blackstock, S. C. *Org. Lett.* **2000**, *2*, 1181.
(20) Li, J. C.; Xue, Z. Q.; Liu, W. M.; Hou, S. M.; Li, X. L.; Zhao, X. Y. *Phys. Lett. A* **2000**, *266*, 441.
(21) Li, J. C.; Liu, W. M.; Xue, Z. Q. *J. Vac. Sci. Technol. B* **2002**, *20*, 673.
(22) Li, J. C.; Kim, K.-Y.; Blackstock, S. C.; Szulczewski, G. J. *Chem. Mater.* **2004**, *16*, 4711.
(23) Ohashi, Y. *Reactivity in Molecular Crystal;* Kodansha: Tokyo, Japan, 1993.
(24) Pope, M.; Swenberg, C. E. *Electronic Processes in Organic Crystals and Polymers;* Oxford: New York, 1999.
(25) Nalwa, H. S. *Handbook of Conductive Molecules and Polymers*; John Wiley & Sons: New York, 1997.
(26) Wang, C. J.; Shim, M. S.; Philippe, G. S. *Science* **2001**, *291*, 2390.
(27) Crone, B. K.; Campbell, I. H.; Davids, P. S.; Smith, D. L. *Appl. Phys. Lett.* **1998**, *73*, 3162.
(28) Zhang, P. C.; Keleshian, A. M.; Sachs, F. *Nature* **2001**, *413*, 428.
(29) Makinen, A. J.; Xu, S.; Zhang, Z.; Diol, S. J.; Gao, Y.; Mason, M. G.; Muenter, A. A.; Mantell, D. A.; Melnyk, A. R. *Appl. Phys. Lett.* **1999**, *74*, 1296.
(30) Collet, E.; Lemee-Cailleau, M.; Cointe, M. B.; Cailleau, H.; Wulff, M.; Luty, T.; Koshihara, S. Y.; Meyer, M.; Toupet, L.; Rabiller, P.; Techert, S. *Science* **2003**, *300*, 612.
(31) Liu, C.-Y.; Bard, A. J. *Nature* **2002**, *418*, 162.
(32) Schneegans, O.; Moradpour, A.; Houze, F.; Angelova, A.; Villeneuve, C. H.; Allongue, P.; Chretien, P. *J. Am. Chem. Soc.* **2001**, *123*, 11486.
(33) Oyamada, T.; Tanaka, H.; Sasabe, H.; Adachi, C. *Appl. Phys. Lett.* **2003**, *83*, 1252.